Applied Physics Letters

RESEARCH ARTICLE | MAY 28 2024

Extracting the electronic structure of light elements in bulk materials through a Compton scattering method in the readily accessible hard x-ray regime

Veenavee Nipunika Kothalawala ; Tejas Guruswamy ; Orlando Quaranta ; Umeshkumar Manibhai Patel ; Lisa Gades ; Keith Taddei ; Andrey Yakovenko ; Meiying Zheng ; Kelsey Morgan ; Joel Weber ; Daikang Yan ; Daniel Swetz ; Ilja Makkonen ; Hemantha Kumar Yeddu ; Arun Bansil ; Uta Ruett ; Antonino Miceli ; Johannes Nokelainen ; Bernardo Barbiellini

Appl. Phys. Lett. 124, 223501 (2024)
https://doi.org/10.1063/5.0207375

Applied Physics Letters ARTICLE pubs.aip.org/aip/apl

Extracting the electronic structure of light elements in bulk materials through a Compton scattering method in the readily accessible hard x-ray regime

Cite as: Appl. Phys. Lett. **124**, 223501 (2024); doi: 10.1063/5.0207375
Submitted: 7 March 2024 · Accepted: 9 May 2024 ·
Published Online: 28 May 2024

View Online Export Citation CrossMark

Veenavee Nipunika Kothalawala,[1,a)] Tejas Guruswamy,[2] Orlando Quaranta,[2] Umeshkumar Manibhai Patel,[2] Lisa Gades,[2] Keith Taddei,[2] Andrey Yakovenko,[2] Meiying Zheng,[1,3] Kelsey Morgan,[4,5] Joel Weber,[4,5] Daikang Yan,[4,6] Daniel Swetz,[4] Ilja Makkonen,[7] Hemantha Kumar Yeddu,[8] Arun Bansil,[9] Uta Ruett,[2] Antonino Miceli,[2] Johannes Nokelainen,[1,9] and Bernardo Barbiellini[1,9]

AFFILIATIONS

[1]Department of Physics, School of Engineering Science, LUT University, FI-53851 Lappeenranta, Finland
[2]X-ray Science Division, Argonne National Laboratory, Lemont, Illinois 60439, USA
[3]L-NESS and Department of Physics, Politecnico di Milano, Como IT 22100, Italy
[4]National Institute of Standards and Technology, Boulder, Colorado 80305, USA
[5]University of Colorado Boulder, Boulder, Colorado 80309, USA
[6]Key Laboratory of Particle Astrophysics, Institute of High Energy Physics, Chinese Academy of Sciences, Beijing, China
[7]Department of Physics, University of Helsinki, P.O. Box 43, FI-00014 University of Helsinki, Helsinki, Finland
[8]Department of Mechanical Engineering, School of Energy Systems, LUT University, FI-53851 Lappeenranta, Finland
[9]Department of Physics, Northeastern University, Boston, Massachusetts 02115, USA

[a)]**Author to whom correspondence should be addressed:** veenavee.kothalawala@lut.fi

ABSTRACT

Our Compton profile measurements of Ti and TiH_2 using readily available hard X-ray radiation at 27.5 keV, detected by both a Hitachi Vortex silicon-drift detector and a high-resolution superconducting transition-edge sensor array, are found to be in excellent accord with state-of-the-art density functional theory based calculations. The spherically averaged difference between the Compton profiles of TiH_2 and Ti is well described by an inverted parabola, supporting an itinerant behavior of the electron gas screening the protons in the Ti matrix. Our experimental approach, validated by two different detectors, extends the applicability of Compton scattering technique to the readily accessible hard x-ray regime (below 30 keV). Our study suggests possibilities for experiments at low-flux bending magnet synchrotron beamlines and paves the way for the development of tabletop Compton experiments with x-ray tubes.

The Compton process (photon in, electron and photon out), a fundamental interaction between x-rays and electrons, offers valuable insights into composition and electronic structure of materials.[1] The Compton x-ray scattering from transition metals, such as Ti, becomes the dominant scattering cross section for an incoming photon energy of approximately 100 keV, as illustrated in Fig. 1. Typical Compton experiments are executed with high-flux beams generated with synchrotron sources.[2] Our objective is to utilize hard x-rays below 30 keV (experimentally accessible even with x-ray tubes[3]) to investigate the influence of light atoms on transition metal compounds for which fluorescence is of very low photon energy and, therefore, suppressed.[4] Previous Compton scattering experiments on titanium and zirconium hydrides have revealed the sensitivity of the Compton profile to hydrogen in these metals.[5–7] Examination of the shape of the Compton profile, influenced by low-momentum electrons in the hydrides, facilitates interpretation through the analysis of Compton profile differences, in

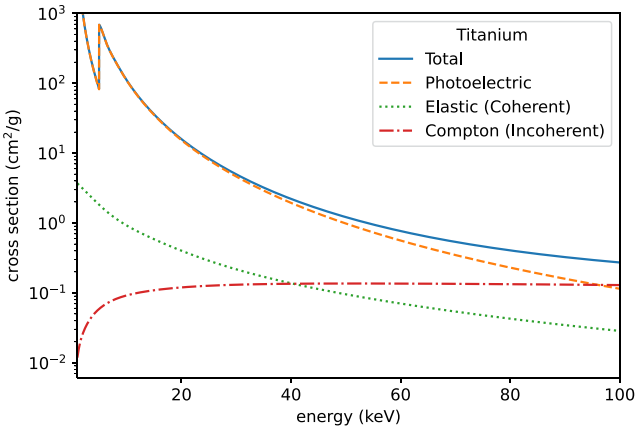

FIG. 1. Calculated x-ray attenuation cross sections for Ti. Various contributions to the total cross section (solid line) are photoelectric, responsible for fluorescence (dashed line); elastic, coherent, or Rayleigh scattering (dotted line); and Compton or incoherent scattering (dash-dotted line). The elastic and Compton contributions for 3*d* metals become equal between 30 and 50 keV.

which many errors are canceled. Combining this experimental strategy with accurate first-principles modeling provides a tool for investigating the impact on electronic properties of light chemical elements in materials.

Our choice of Ti and TiH_2 for this study is motivated for several reasons. Ti is well known to exhibit a remarkable capacity to absorb hydrogen.[8,9] Hydrogen plays a crucial role in energy storage applications[10] and in including fascinating properties in transition-metal hydrides, including superconductivity.[11,12] Ti alloys are used extensively in structural components of the hydrogen infrastructure. Our study thus represents a significant advancement in the applications of the Compton scattering technique as well as in the understanding of the electronic structure of TiH_2.

We collected spectroscopic data from a Ti metal foil with HCP crystal structure, with dimensions $10 \times 10 \times 0.5\,mm^3$, and TiH_2 powder, retained in a Kapton film of approximately the same outer dimensions. The samples were illuminated by a 27.5 keV monochromatic x-ray beam at the 1-BM bending magnet at the Advanced Photon Source (APS) using a Si(111) double-crystal monochromator. All samples were mounted free-standing in the beam path (in air) under a 45 degree angle to the incident beam of 5 mm (horizontal) and 1 mm (vertical). This angled the sample toward two detectors also in the horizontal plane, both measuring simultaneously—A 96-pixel superconducting transition-edge sensor (TES) array (fabricated at NIST-Boulder) was placed almost perpendicular at a 87.5 degree scattering angle respective to the incoming photon beam and a single-element Hitachi Vortex silicon-drift detector (SDD) at 138 degree in backscattering geometry. The scattering angles were determined by the photon energy of the Compton scattering. The distance from the sample to the active surface of either detector was 250 mm. In order to reduce the proportion of detected photons from lower-energy fluorescence relative to higher-energy Compton scattering, two layers of 0.1 mm thick Al foil were placed in front of each detector. Each sample was measured for approximately 6 h at a constant count rate, allowing for the collection of $> 5 \times 10^6$ integrated photon counts by the TES array and $> 4 \times 10^7$ integrated counts by the SDD. We estimate from ion-chamber readings the total flux incident on the sample as 2.5×10^{10} photons/second, which is also achievable with sealed x-ray tube sources.[13,14] Further description of a similar Compton experimental setup and TES instrument is given in Patel *et al.*[15]

TABLE I. Estimated total momentum resolution σ_p, and the associated contributions from the energy width of the incoming x-ray beam, the energy resolution of the detector, and the angular spread associated with the experimental geometry, for the two different detectors used. Root-mean square values are given.

Detector	$\sigma_{E_{in}}$(eV)	$\sigma_{E_{out}}$(eV)	$\sigma_\theta(^\circ)$	σ_p(a.u.)
TES	1.75	14	2.04	0.19
SDD	1.75	130	0.88	0.40

Determining the central energy of the Compton peak was aided by fitting a model consisting of a Laplace (double-exponential) added to a Gaussian function, an approximation of the convoluted function. Van Gysel *et al.*[16] found to be the best match to a typical Compton profile shape. Contributions to the total experimental momentum resolution σ_p for each detector were estimated as in Table I. Note that the σ values quoted here and the full-width-at-half-maximum (FWHM) values are related by $\mathrm{FWHM} = 2\sqrt{2\ln(2)}\,\sigma$. Detector energy resolutions were obtained by fitting a Gaussian to the elastic peak in the measured spectrum. The incident energy resolution was set to $\Delta E/E = 1.5 \times 10^{-4}$. We found the total momentum resolution for the TES detector to be dominated by the angular contribution due to its positioning at approximately 90° and its larger field of view (wider than in Patel *et al.*[15] due to different collimation), while for the SDD, the overall momentum resolution was dominated by the detector energy resolution.

Theoretical models of the Compton profiles were convoluted with a Gaussian function of width $\sigma = \sigma_p$ prior to comparison with the experimental data. The experimental profiles were normalized so that the total areas between $p_z = -4$ to 4 a.u. were equal to the area over the same range of the corresponding theoretical density functional theory (DFT)-based profiles, which were themselves normalized over a large momentum range so that their total areas were equal to the total number of electrons involved ($Z = 22$ for Ti and $Z = 24$ for TiH_2).

The TES array data were further scaled up by 5% to account for the presence of Ti *L*-line escape peaks overlapping the Compton peak. No multiple-scattering, background subtraction, or other corrections to the measured profiles were applied, and no other free parameters were used in the analysis. The probability of multiple scattering is proportional to the optical thickness of the sample[17]—approximately 1.5 attenuation lengths in our case—and so will affect our measured profiles. However, since our samples have the similar thickness and similar density, and the corrections due to multiple scattering are broad relative to the main Compton profile (smoothing over differences due to the sample composition), we expect multiple-scattering contributions to largely cancel out when we consider the difference Compton profiles. A powder x-ray diffraction measurement of the TiH_2 sample returned a lattice parameter value of 4.450 Å compared to the literature value[18] of 4.41 AA and supported the FCC structure used in our modeling, see Fig. S1 in the supplementary material.

The collected spectra were transformed into momentum space via the formulation of Ribberfors.[19] Within the *impulse approximation*,[20] the double-differential cross section is

$$\frac{\mathrm{d}^2\sigma}{\mathrm{d}\Omega\mathrm{d}E} = F \cdot J(p_z), \tag{1}$$

where the explicit form of F that accounts for relativistic effects is given by Ribberfors.[19] Failure of the impulse approximation produces an asymmetry in the experimental Compton profile as shown in Huotari *et al.*[21] We find only a very slight asymmetry about $p_z = 0$ in our measured Compton profiles, which we attribute to the background and not to the Compton profile itself, as illustrated in Fig. S2 in the supplementary material. The Compton profile $J(p_z)$ is given in terms of the ground-state electron momentum density $\rho(\mathbf{p})$ by the following formula:[22]

$$J(p_z) = \int\int \rho(\mathbf{p})\mathrm{d}p_x\mathrm{d}p_y, \tag{2}$$

where $\mathbf{p} = (p_x, p_y, p_z)$ is the electron momentum and p_z is taken to lie along the direction of the scattering vector. The electron momentum density can be expressed as

$$\rho(\mathbf{p}) = \sum_j^{\mathrm{occ}} \left| \int \Psi_j(\mathbf{r}) \exp(-i\mathbf{p}\cdot\mathbf{r})\mathrm{d}^3\mathbf{r} \right|^2, \tag{3}$$

where an independent particle approximation is assumed.

Core electron states of Ti and H were described by Hartree–Fock (HF) orbitals provided by Biggs *et al.*[23] Valence electronic structure modifications of Ti and TiH_2 were obtained via *ab initio* DFT-based calculations using the projector-augmented-wave (PAW) method[24] as implemented in the Vienna *Ab initio* Simulation Package (VASP)[25,26] with an energy cutoff of 520 eV. Exchange-correlation effects were treated using the generalized gradient approximation (GGA) functional parameterized by Perdew, Burke, and Ernzerhof (PBE).[27] A variant, PBE functional revised for solids (PBEsol),[28] can improve the description of certain electronic properties. However, Sharma *et al.*[29] showed that the corrections for the Compton profiles using PBEsol (compared to local density approximation and therefore to PBE) are marginal. Therefore, we opted to use PBE, which is preferable in general over PBEsol. The crystal structure and the ionic positions were optimized using a force convergence criterion of 0.01 eV/Å for each atom, along with a total energy tolerance of 10^{-5} eV. For the Ti metal, we employed the standard HCP structure with a 2-atom primitive cell, characterized by $a, b = 2.94$ Å and $c = 4.64$ Å. For TiH_2, we used the FCC structure proposed by Shanavas *et al.*,[11] with a unit cell containing 12 atoms and an equilibrium lattice constant a of 4.41 AA. The Brillouin zone was sampled using a uniform Γ-centered $7 \times 7 \times 7$ k-point grid. Within the DFT framework, the spherically averaged electron momentum density was calculated with Kohn–Sham orbitals following the methodology of Makkonen *et al.*[30]

In addition to atomic Hartree–Fock and DFT calculations, we consider two simple models to gain physical insight into the fate of the electron associated with the hydrogen atom. In the *screened model*,[6] the influence of the host metal is incorporated by screening the proton with an effective charge Z. The wavefunction of the electron screening the proton is then given by $\psi(r) = Z^3/\pi \exp(-Zr)$, and the corresponding Compton profile (normalized to Z) is

$$J(p_z) = \frac{8Z^5}{3\pi(p_z^2 + Z^2)^3}. \tag{4}$$

In the *free electron model*,[2] the electrons donated by the H atoms form a non-interacting free-electron gas. In this case, the electrons occupy all available energy levels up to the Fermi energy E_F. Since the energy band is given by $E(p) = p^2/2m$, the occupied states form the Fermi sphere, with the radius of the Fermi momentum $p_F = \sqrt{2mE_F}$, and the Compton profile per electron is given by

$$J(p_z) = \begin{cases} 3(p_F^2 - p_z^2)/4p_F^3, & \text{if } |p_z| < p_F, \\ 0, & \text{otherwise.} \end{cases} \tag{5}$$

Figure 2 displays our raw SDD and TES spectra, where the contribution from fluorescence, Rayleigh, and Compton scattered radiation is observable. These spectra are based on broadband energy-dispersive instruments in which the entire energy range is recorded in one measurement. Inelastic Compton scattering leads to a decrease in the energy of the x-ray, which depends on the scattering angle, and since our two detectors were at different positions, the Compton peaks lie at different energies in the measured spectra. Even with the Al foils acting as a high-pass filter, a significant proportion of the total counts recorded are fluorescence, primarily from Ti in the sample, but also some Cu and Zn background from the sample mount and detector housing. In a synchrotron environment, we are photon-rich and primarily limited by our detector maximum count rates; therefore, it is beneficial to filter out the scattered photons that do not contribute to the experiment. In a benchtop setup, for example, where an x-ray tube is used for illumination, one is more likely to be limited by the source flux, and filters may not be needed.

Compton profiles measured by the TES and SDD and transformed into momentum space are shown in Fig. 3. We compare the measured data to the atomic model of Biggs *et al.*[23] and the DFT

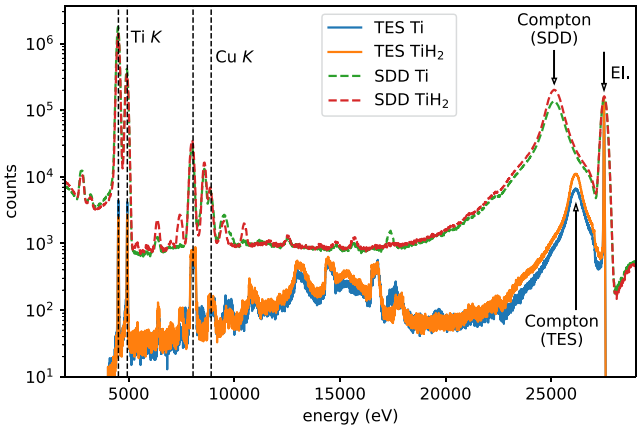

FIG. 2. Broadband x-ray emission spectra of solid metal Ti (blue) and TiH_2 powder (behind Kapton) (orange), as measured by a superconducting transition-edge sensor (TES) array (solid) and a silicon-drift detector (SDD) (dashed). The elastic line at 27.5 keV and the Compton peaks are labeled with arrows. Compton peaks lie at different energies in the two detectors because different scattering angles were used: (87.5° for the TES and 138° for the SDD). Also labeled (dashed vertical lines) are selected prominent fluorescence peaks: Ti *K*-lines from the sample and Cu *K*-lines from the sample environment.

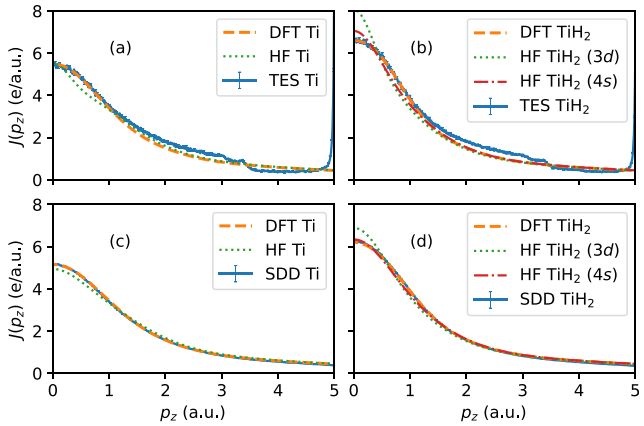

FIG. 3. Compton profiles of (a) Ti and (b) TiH_2 measured with a superconducting transition-edge sensor array (solid, in both plots) compared with theoretical models convoluted with a Gaussian of width $\sigma = 0.19$ a.u. Compton profiles of (c) Ti and (d) TiH_2 measured with a silicon-drift detector (solid, in both plots), compared with theoretical models convoluted with a Gaussian of width $\sigma = 0.4$ a.u. Theoretical plots are based on our DFT computations (dashed) and the free-atom Hartree–Fock model (dotted), with two possible electronic configurations of TiH_2 (see main text). Experimental data are plotted with Poisson ($\sqrt{N}$) error bars, in (a) and (b) only every three points for clarity.

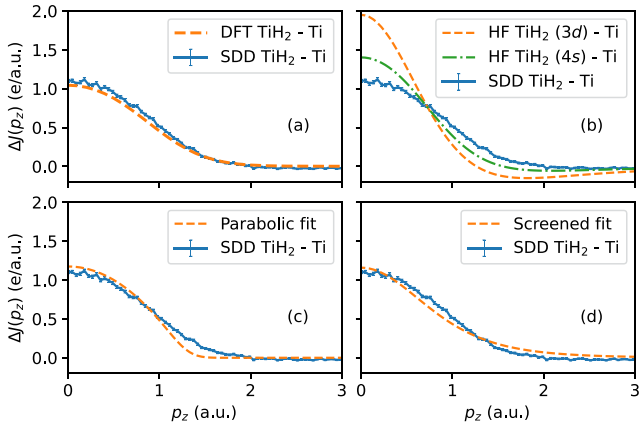

FIG. 4. Difference profile $\Delta J(p_z)$ [$TiH_2 - Ti$] measured with a silicon-drift detector (solid, in all plots), compared to the corresponding calculations: (a) using the DFT methods of this paper (dashed); (b) using two possible electronic configurations of TiH_2 (see main text) and the free-atom Hartree–Fock model (dashed and dash-dotted); (c) using a free-electron model parabolic fit (dashed); and (d) using the screened-atomic model (dashed). Theoretical calculations have been convoluted with a Gaussian of width $\sigma = 0.4$ a.u. Experimental data are plotted with 1σ error bars.

model of this paper. The atomic model used for Ti is [Ar] $3d^3 4s^1$, as suggested by Berggren *et al.*[31] In the atomic models of TiH_2, we assume either the 3*d* or the 4*s* orbitals of Ti donate the first electron to the hydrogen atoms, resulting in [Ar] $3d^1 4s^1$ or [Ar] $3d^2$ configurations, referred to as TiH_2-3*d* and TiH_2-4*s*, respectively. Clearly, the latter provides a better agreement with the experiment. Further, it is evident that DFT significantly improves the agreement between the model and experiment compared to the models involving only atomic orbitals.

Once we account for the experimental setup and the associated uncertainties, the agreement between the DFT-based results and the SDD measurements for Ti and TiH_2 is excellent, without invoking any free parameters. The spectra collected from the higher-energy-resolution TES detector also exhibits very good agreement with theory in the central region of the Compton profiles of both Ti and TiH_2, but the peak shape appears slightly compressed, in that the peak height is slightly smaller relative to the wings. This discrepancy could be attributed to the detector, which is still under development, and/or to complications resulting from the mixing of Ti *L*-edge escape peaks visible at approximately $p = 3.5$ a.u. with the Compton profile. Some disagreement is also expected as we have not performed any background subtraction. In this energy range, the largest contribution to the background is Bremsstrahlung radiation from photoelectrons. Due to its spectral shape, the magnitude of the Bremsstrahlung contribution in the Compton peak region must be no larger than the magnitude of the total background at lower energies, e.g., at 20 keV, which allows us to estimate an upper bound on the ratio of Bremsstrahlung to Compton counts of 6% in our measurements. This is likely an overestimate given published calculations of ratios below 1% for higher incident energies and atomic numbers.[32] Overall, the spherically averaged Compton profiles of TiH_2 and Ti provide a reasonable match between theory and experiment.

The agreement between theory and experiment is further improved when we consider the difference $\Delta J(p_z)$ between the profiles of TiH_2 and Ti ($TiH_2 - Ti$), see Figs. 4 and 5 for the SDD and TES detector, respectively. The $\Delta J(p_z)$ profile allows one to focus on the modifications to the electronic structure in going from Ti to TiH_2 (Ref. 6) because the core contribution and several systematic corrections to the experimental spectra (e.g., background, energy dependence of the scattering cross section, detector efficiency, absorption, and multiple-scattering corrections), are largely subtracted out.

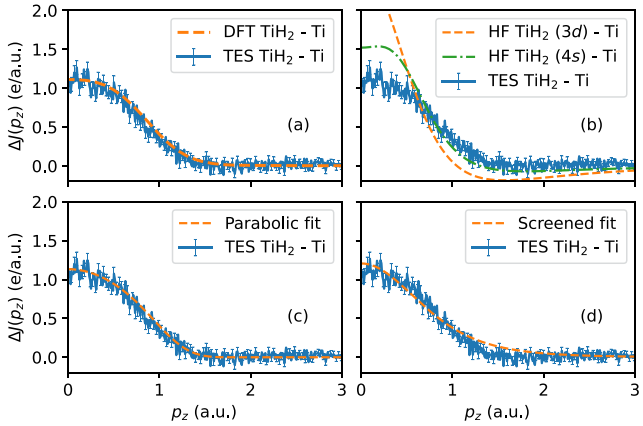

FIG. 5. Difference profile $\Delta J(p_z)$ [$TiH_2 - Ti$] measured with a superconducting transition-edge sensor array (solid, in all plots), compared with the corresponding calculations (a) using the DFT methods of this paper (dashed); (b) using two possible electronic configurations of TiH_2 (see main text), and the free-atom Hartree–Fock model (dashed and dash-dotted); (c) using a free-electron model parabolic fit (dashed); and (d) using the screened-atomic model (dashed). Theoretical calculations have been convoluted with a Gaussian of width $\sigma = 0.19$ a.u. Experimental data are plotted with 1σ error bars, every three points for clarity.

Figures 4 and 5 indeed show very similar results for both detectors. The agreement with DFT now remains excellent across the entire momentum range for both detectors, and other models do not perform as well as the DFT. Notably, the rapid fluctuations in the experimental profiles in Fig. 5 fall within the error bars. Interestingly, the density of states of Ti and TiH_2 (supplementary material) displays a free electron-like character. However, the Compton profile difference, as predicted by DFT, can still be approximated by an inverted parabolic shape given by Eq. (5) with fitted Fermi momentum $p_F = 1.3$ a.u. The electron gas described by $\Delta J(p_z)$ is responsible for screening the protons embedded in the Ti matrix and forms the hydrogen-induced 1*s* valence band, discussed by Fujimori and Tsuda,[33] which accommodates two electrons per titanium atom in TiH_2. (The partial density of states and the contribution of the hydrogen-induced 1*s* valence band are discussed in the supplementary material.) We can visualize the electronic states associated with this band by considering the $TiH_2 - Ti$ difference of the charge densities in real space. Finally, we perform a Bader charge analysis,[34,35] which shows that the value of 1.72 electrons on the H site is consistent with the charge parameter $Z = 1.6$ used in the screened atomic model by Alexandropoulos *et al.*[6]

This study addresses questions identified in previous studies by Alexandropoulos *et al.*[6] on the spherically averaged difference Compton profile of TiH_2 and Ti, where the simple hydrogen atom model with effective charge $Z = 1$ was shown to fail in describing the experimental spectrum. The model with $Z < 1$ proved worse in predicting the difference Compton profile. However, a screened model with $Z = 1.6$ and a model in which the electron of the hydrogen was assumed to occupy the electronic band of Bakalis *et al.*[5] yielded better agreement with experiment. Here, we show that state-of-the-art DFT-based calculations of Compton profiles of Ti and TiH_2 provide an excellent description of the measured difference Compton profiles without invoking any free parameters.

Our experimental approach is robust across measurement by two very different detectors—a Hitachi Vortex SDD and a high-resolution superconducting TES. It also offers possibilities for exploiting the Compton scattering techniques by using the readily accessible hard x-ray regime (below 30 keV) at low-flux synchrotron bending magnet beamlines. Finally, our study indicates the value of developing a tabletop Compton spectrometer as a laboratory-based spectroscopic tool for investigating electronic structures of materials. Existing portable x-ray fluorescence spectroscopy techniques make use of the intensity of the Compton peak to determine light-element content in the sample, including for calibration, e.g., Fig. 3 in of Laperche and Lemière.[36] Our work demonstrates that in Compton profiles measured with similar incident energies and resolutions, information about electronic structure is also available. We also find focusing on difference profiles greatly reduces the complexity of analysis and experimental data corrections needed, again improving accessibility. This advancement holds promise for a wide range of applications[37] in materials science, environmental analysis, and biomedical research, among other areas.

See the supplementary material for further experimental and computational details, including x-ray diffraction patterns, asymmetry of Compton profiles, analysis of the density of states, charge density distribution, Bader charge analysis, and convergence testing.

The work at LUT was supported by the INERCOM platform. The work at Northeastern benefited from the Massachusetts Technology Collaborative through Award No. 22032 and Northeastern University's Advanced Scientific Computation Center. This research used resources of the Advanced Photon Source (APS) and Center for Nanoscale Materials (CNM), U.S. Department of Energy (DOE) Office of Science user facilities, and is based on the work supported by Laboratory Directed Research and Development (LDRD) funding from the Argonne National Laboratory, provided by the Director, Office of Science, of the U.S. DOE under Contract No. DE-AC02-06CH11357. Data were collected at the x-ray Science Division's bending magnet beamline 1-BM-C at APS. The authors wish to acknowledge CSC–IT Centre for Science, Finland, for computational resources.

AUTHOR DECLARATIONS

Conflict of Interest

The authors have no conflicts to disclose.

Author Contributions

Veenavee Nipunika Kothalawala: Conceptualization (equal); Data curation (equal); Formal analysis (equal); Investigation (equal); Methodology (equal); Validation (equal); Visualization (equal); Writing – original draft (equal); Writing – review & editing (equal). **Tejas Guruswamy:** Conceptualization (equal); Data curation (equal); Formal analysis (equal); Investigation (equal); Methodology (equal); Visualization (equal); Writing – original draft (equal). **Orlando Quaranta:** Conceptualization (equal); Formal analysis (equal); Investigation (equal); Methodology (equal); Writing – review & editing (equal). **Umeshkumar Manibhai Patel:** Conceptualization (equal); Formal analysis (equal); Investigation (equal); Methodology (equal); Writing – original draft (equal). **Lisa Gades:** Conceptualization (equal); Formal analysis (equal); Investigation (equal); Methodology (equal); Writing – review & editing (equal). **Keith Taddei:** Conceptualization (equal); Formal analysis (equal); Investigation (equal); Methodology (equal); Writing – review & editing (equal). **Andrey Yakovenko:** Formal analysis (equal); Investigation (equal); Methodology (equal); Writing – review & editing (equal). **Meiying Zheng:** Conceptualization (equal); Investigation (equal); Methodology (equal); Writing – review & editing (equal). **Kelsey Morgan:** Investigation (equal); Methodology (equal); Writing – review & editing (equal). **Joel Weber:** Investigation (equal); Methodology (equal); Writing – review & editing (equal). **Daikang Yan:** Investigation (equal); Methodology (equal); Writing – review & editing (equal). **Daniel Swetz:** Investigation (equal); Methodology (equal); Writing – review & editing (equal). **Ilja Makkonen:** Conceptualization (equal); Methodology (equal); Software (equal); Writing – original draft (equal); Writing – review & editing (equal). **Hemantha Kumar Yeddu:** Writing – original draft (equal); Writing – review & editing (equal). **Arun Bansil:** Conceptualization (equal); Funding acquisition (equal); Investigation (equal); Methodology (equal); Writing – original draft (equal); Writing – review & editing (equal). **Uta Ruett:** Conceptualization (equal); Funding acquisition (equal); Investigation (equal); Methodology (equal); Supervision (equal); Writing – original draft (equal); Writing – review & editing (equal). **Antonino Miceli:** Conceptualization (equal); Investigation (equal); Methodology (equal);

Writing – original draft (equal); Writing – review & editing (equal). **Johannes Nokelainen:** Conceptualization (equal); Investigation (equal); Methodology (equal); Writing – original draft (equal); Writing – review & editing (equal). **Bernardo Barbiellini:** Conceptualization (equal); Formal analysis (equal); Funding acquisition (equal); Investigation (equal); Methodology (equal); Supervision (equal); Writing – original draft (equal); Writing – review & editing (equal).

DATA AVAILABILITY

The data that support the findings of this study are available from the corresponding author upon reasonable request.

REFERENCES

[1]M. Cooper, P. Mijnarends, N. Shiorani, N. Sakai, and A. Bansil, *X-Ray Compton Scattering* (Oxford University Press, Oxford, 2004), pp. 31–39.
[2]B. Barbiellini and A. Bansil, "Scattering techniques, Compton," in *Encyclopedia of Condensed Matter Physics (Second Edition)*, 2nd ed., edited by T. Chakraborty (Academic Press, Oxford, 2024), pp. 173–186.
[3]L. O'Neil, D. Catling, and W. Elam, "Optimized Compton fitting and modeling for light element determination in micro-X-ray fluorescence map datasets," Nucl. Instrum. Methods Phys. Res., Sect. B **436**, 173–178 (2018).
[4]E. D. Isaacs, A. Shukla, P. M. Platzman, D. R. Hamann, B. Barbiellini, and C. A. Tulk, "Covalency of the hydrogen bond in ice: A direct X-Ray measurement," Phys. Rev. Lett. **82**, 600–603 (1999).
[5]N. C. Bacalis, N. I. Papanicolaou, and D. A. Papaconstantopoulos, "Theoretical Compton profiles due to valence electrons of Ti and TiH_2," J. Phys. F: Met. Phys. **16**, 1471 (1986).
[6]N. Alexandropoulos, I. Theodoridou, and M. Cooper, "Compton scattering studies of hydrogen in titanium," J. Phys. C: Solid State Phys. **20**, 1201 (1987).
[7]N. Alexandropoulos, S. Danakas, K. Kotsis, and N. Papanicolaou, "Difference Compton profiles of Zr and ZrH_2," Solid State Commun. **92**, 453–457 (1994).
[8]S. X. Tao, P. H. L. Notten, R. A. van Santen, and A. P. J. Jansen, "Density functional theory studies of the hydrogenation properties of Mg and Ti," Phys. Rev. B **79**, 144121 (2009).
[9]Y. Liu, Y. Gong, Y. Wang, Y. Jiang, C. Shen, X. Zhou, and X. Long, "Structures and stabilities of titanium hydride surfaces: A first-principles thermodynamic study," J. Mater. Sci. **58**, 12236–12250 (2023).
[10]L. Schlapbach and A. Züttel, "Hydrogen-storage materials for mobile applications," Nature **414**, 353–358 (2001).
[11]K. V. Shanavas, L. Lindsay, and D. S. Parker, "Electronic structure and electron-phonon coupling in TiH_2," Sci. Rep. **6**, 28102 (2016).
[12]J. Zhang, J. M. McMahon, A. R. Oganov, X. Li, X. Dong, H. Dong, and S. Wang, "High-temperature superconductivity in the Ti-H system at high pressures," Phys. Rev. B **101**, 134108 (2020).
[13]V. Honkimäki, J. Sleight, and P. Suortti, "Characteristic X-ray flux from sealed Cr, Cu, Mo, Ag and W tubes," J. Appl. Crystallogr. **23**, 412–417 (1990).
[14]O. Hemberg, M. Otendal, and H. M. Hertz, "Liquid-metal-jet anode electron-impact x-ray source," Appl. Phys. Lett. **83**, 1483–1485 (2003).
[15]U. Patel, T. Guruswamy, A. J. Krzysko, H. Charalambous, L. Gades, K. Wiaderek, O. Quaranta, Y. Ren, A. Yakovenko, U. Ruett, and A. Miceli, "High-resolution Compton spectroscopy using X-ray microcalorimeters," Rev. Sci. Instrum. **93**, 113105 (2022).
[16]M. Van Gysel, P. Lemberge, and P. Van Espen, "Description of Compton peaks in energy-dispersive X-ray fluorescence spectra," X-Ray Spectrom. **32**, 139–147 (2003).
[17]P. Fajardo, V. Honkimäki, T. Buslaps, and P. Suortti, "Experimental validation of multiple scattering calculations with high energy X-ray photons," Nucl. Instrum. Methods Phys. Res., Sect. B **134**, 337–345 (1998).
[18]A. Jain, S. P. Ong, G. Hautier, W. Chen, W. D. Richards, S. Dacek, S. Cholia, D. Gunter, D. Skinner, G. Ceder, and K. A. Persson, "Commentary: The Materials Project: A materials genome approach to accelerating materials innovation," APL Mater. **1**(1), 011002 (2013).
[19]R. Ribberfors, "Relationship of the relativistic Compton cross section to the momentum distribution of bound electron states," Phys. Rev. B **12**, 2067–2074 (1975).
[20]I. G. Kaplan, B. Barbiellini, and A. Bansil, "Compton scattering beyond the impulse approximation," Phys. Rev. B **68**, 235104 (2003).
[21]S. Huotari, K. Hämäläinen, S. Manninen, A. Issolah, and M. Marangolo, "Asymmetry of Compton profiles," J. Phys. Chem. Solids **62**, 2205–2213 (2001).
[22]J. Nokelainen, B. Barbiellini, J. Kuriplach, S. Eijt, R. Ferragut, X. Li, V. Kothalawala, K. Suzuki, H. Sakurai, H. Hafiz *et al.*, "Identifying redox orbitals and defects in lithium-ion cathodes with Compton scattering and positron annihilation spectroscopies: A review," Condens. Matter **7**, 47 (2022).
[23]F. Biggs, L. Mendelsohn, and J. Mann, "Hartree-Fock Compton profiles for the elements," At. Data Nucl. Data Tables **16**, 201–309 (1975).
[24]P. E. Blöchl, "Projector augmented-wave method," Phys. Rev. B **50**, 17953–17979 (1994).
[25]G. Kresse and J. Furthmüller, "Efficiency of ab-initio total energy calculations for metals and semiconductors using a plane-wave basis set," Comput. Mater. Sci. **6**, 15 (1996).
[26]G. Kresse and D. Joubert, "From ultrasoft pseudopotentials to the projector augmented-wave method," Phys. Rev. B **59**, 1758–1775 (1999).
[27]J. Perdew, K. Burke, and M. Ernzerhof, "Generalized gradient approximation made simple," Phys. Rev. Lett. **77**, 3865–3868 (1996).
[28]J. P. Perdew, A. Ruzsinszky, G. I. Csonka, O. A. Vydrov, G. E. Scuseria, L. A. Constantin, X. Zhou, and K. Burke, "Restoring the density-gradient expansion for exchange in solids and surfaces," Phys. Rev. Lett. **100**, 136406 (2008).
[29]K. Sharma, J. Sahariya, and B. Ahuja, "Electronic structure, optical properties and Compton profiles of RuO_2: Performance of PBEsol exchange–correlation approximation," J. Alloys Compd. **645**, 414–420 (2015).
[30]I. Makkonen, M. Hakala, and M. Puska, "Calculation of valence electron momentum densities using the projector augmented-wave method," J. Phys. Chem. Solids **66**, 1128–1135 (2005).
[31]K.-F. Berggren, S. Manninen, and T. Paakkari, "Electron momentum distribution in titanium and the renormalized-free-atom model," Phys. Rev. B **8**, 2516 (1973).
[32]U. Mittal, B. Sharma, and R. Kothari, "Bremsstrahlung contribution in Compton scattering from heavy metals," Z. Naturforsch. A **48**, 348–351 (1993).
[33]A. Fujimori and N. Tsuda, "Electronic structure of non-stoichiometric titanium hydride," J. Less Common Met. **88**, 269–272 (1982).
[34]W. Tang, E. Sanville, and G. Henkelman, "A grid-based Bader analysis algorithm without lattice bias," J. Phys.: Condens. Matter **21**, 084204 (2009).
[35]M. Yu and D. R. Trinkle, "Accurate and efficient algorithm for Bader charge integration," J. Chem. Phys. **134**, 064111 (2011).
[36]V. Laperche and B. Lemière, "Possible pitfalls in the analysis of minerals and loose materials by portable XRF, and how to overcome them," Minerals **11**, 33 (2020).
[37]A. Frydrych and K. Jurowski, "Portable x-ray fluorescence (pXRF) as a powerful and trending analytical tool for in situ food samples analysis: A comprehensive review of application-state of the art," TrAC Trends Anal. Chem. **166**, 117165 (2023).